

1

Visualization of the Seismic Ambient Noise Spectrum

DANIEL E. MCNAMARA AND RICHARD I. BOAZ

Abstract

In this chapter we visualize and review the major components of the Earth's ambient seismic noise spectrum. Short-period noise is dominated by human activity, while mid- and long-period noise is dominated by effects from ocean waves. For earthquake-monitoring and detection purposes it is important to know the seismic ambient noise levels experienced by a network of seismic stations. To make this assessment we describe the probability density function of power spectral density (PSDPDF) method in full. We discuss both operational and research applications of ambient seismic noise analysis, concluding with software and data resources available to students and researchers interested in studying the spectral characteristics of ambient seismic noise.

1.1 Introduction to Ambient Seismic Noise

For many seismologists, the study of seismic ambient noise aims to improve the fidelity of signals generated from events of interest such as earthquakes and nuclear explosions. In fact, the study of seismic noise illuminates a variety of signals which can reveal characteristics of a broad range of sources that include ocean waves (e.g., Gutenberg, 1936; Bromirski, 2009; Díaz, 2016) (see Chapter 3), climate (Aster et al., 2008, 2010; Ebeling, 2012), glaciers (O'Neel et al., 2007; Walter et al., 2010; Ekström et al., 2003, 2006), ship wakes, wind waves (McNamara et al., 2011), urban areas (e.g., McNamara and Buland, 2004), and even rugby matches (e.g., Boese et al., 2015). For operational seismology, the study of seismic noise can provide information about the performance of seismic instrumentation, recording station construction designs, and the quality of metadata (Hutt et al., 2017; McNamara et al., 2005, 2009; Ringler et al., 2010, 2015).

With advances in modern broadband instrumentation over the past few decades, theoretical understanding of seismic ambient noise has rapidly improved, and the number of its applications has increased dramatically. As you will see throughout the chapters of this book, seismic ambient noise/signals have been used to study many natural climate and environmental processes and improve the resolution of earth velocity and attenuation models (e.g., Bensen et al., 2008) (see Chapter 5). In this chapter we will use the standard seismology nomenclature and refer to any non-earthquake signal as noise. However, as we will demonstrate, noise is often a very useful signal.

1.1.1 Motivation to Visualize the Ambient Seismic Noise Spectrum

For earthquake-monitoring and detection purposes it is important to know the seismic ambient noise levels experienced by a network of seismic stations. Detailed frequency (1/period) dependent observations can contribute to improved seismic station and network design, which will in turn improve the detection of earthquakes and other seismic sources of interest, such as nuclear explosions. Beginning with the publication of high and low seismic background displacement curves of Brune and Oliver (1959) and Frantti et al. (1962), Earth noise models that have been used as baselines for evaluating seismic station site characteristics and construction methods, instrument quality, and environmental seismic noise sources. Later studies compared seismic noise models for different tectonic regions such as island arcs versus stable continental landmasses using more modern digital seismic instrumentation (Peterson, 1993; Stutzmann et al., 2000; Berger et al., 2004; Butler et al., 2004; Wilson et al., 2002; Bahavar and North, 2002; Reif et al., 2002). Using long-term broadband records from stations within the GSN, the standard Peterson (1993) new low-noise model (NLNM) (Figure 1.1a) was constructed by removing earthquakes and other transient signals from the seismic records to identify the minimum noise levels representative of quiet periods at continental interior seismic stations distributed around the world. The new high-noise model (NHNM) (Figure 1.1a) was constructed with the same processing methods, though using mostly island-based stations within the GSN (Peterson, 1993).

While it may be scientifically interesting to determine the absolute quietest noise levels achieved by a network, more recent studies find that these low noise levels are generally very low probability occurrences (< 10%) and do not closely track the significantly higher probability power levels. In fact, statistical median (50%) noise levels are as much as 25 dB above short-period (0.1–1 s) minimums (Figure 1.1a). For earthquake monitoring, it is important to know the distribution of ambient seismic noise in a probabilistic sense since noise significantly impacts magnitude detection threshold (e.g., McNamara et al., 2016).

Visualization of the Seismic Ambient Noise Spectrum

3

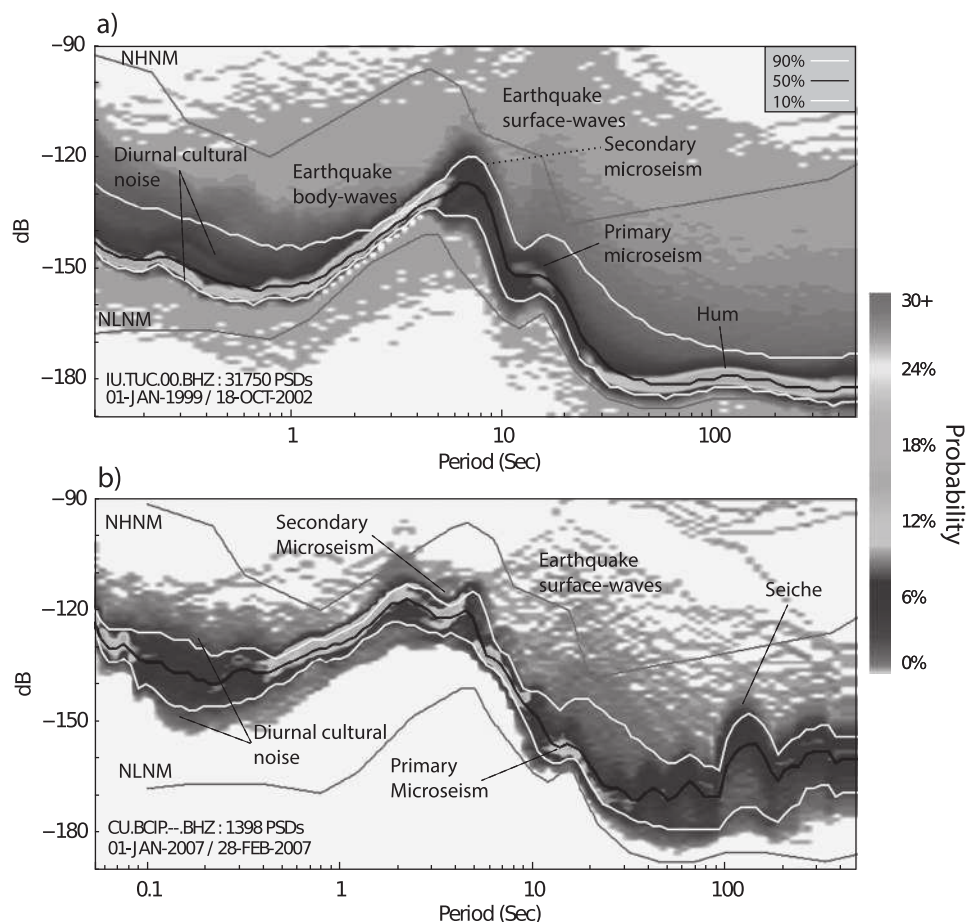


Figure 1.1. Major components of the seismic ambient noise spectrum. Red to green colors (in the color version; lighter grey colors in the greyscale version) indicate the highest probability seismic ambient noise power levels at each period. Baseline statistics shown as solid lines (10th% lower white line, 50th% black line and 90th% upper white line). New low-noise model (NLNM) and new high-noise model (NHNM) shown as gray lines (Peterson, 1993). (a) PSDPDF computed using data from a GSN station in Tucson, Arizona (IU.TUC.00.BHZ, 31,750 PSDs, 01-JAN-99-18-OCT-02). (b) PSDPDF computed using data from a GSN station on Isla Barro Colorado, Panama (CU.BCIP.00.BHZ, 1,398 PSDs, 01-JAN-07-28-FEB-07). (A black-and-white version of this figure appears in some formats. For the color version, please refer to the plate section.)

For example, many seismic stations are surrounded by urban areas and have considerably higher median noise levels at periods important to earthquake detection (0.1–1 s), and thus will significantly impact earthquake body and surface wave-wave detection capabilities (Figure 1.1). This is the principal reason that the noise levels of the NLNM have such low probabilities of occurrence for stations

worldwide (Figure 1.1). For many stations such low levels of noise are unattainable, suggesting that for routine earthquake-monitoring purposes a global noise threshold based on higher probability noise levels is more useful.

There is no need to screen for system transients, earthquakes or general data artifacts since they map into a background, low-probability level of occurrence. Examination of artifacts related to station operation and episodic seismic noise, which would have been removed using past methods, allows us to estimate both the overall station quality and a baseline level that is specific to each site. This renders the results of this analysis useful for characterizing the performance of a seismic sensor, detecting operational problems within the recording system, and evaluating the overall quality of data produced by a particular station. The main advantage of the probability density function of power spectral density (PSDPDF) is the probabilistic view across a broad spectrum of periods. This allows for long-term assessment of the seismic instrument performance and research on the major sources of ambient seismic noise.

1.1.2 Sources of the Ambient Seismic Noise Spectrum

The broadband seismic ambient noise spectrum is multimodal with distinctly different physical mechanisms transferring energy into the solid Earth as seismic waves (e.g., Figure 1.1a). The broadband PSDPDF of ambient noise at a seismic station will thus describe noise coming from several different sources predominantly from machinery, water waves, and atmospheric oscillations.

At short periods (0.1–1 s) ambient noise power levels are generally dominated by human-generated (i.e., “cultural”) seismic energy radiated from the electrical grid, cars, trains, and machinery within a few kilometers of the recording station. Intermediate periods (1–30 s) are dominated by microseisms, that can be many orders of magnitude higher in power than other parts of the seismic spectrum. Long-period (30–500 s) signals are generally caused by ocean infragravity waves generated by storm-forced, shoreward-directed winds, commonly referred to as “Hum.” These major noise source characteristics are discussed in detail in Section 1.3.

This chapter provides the reader with the following: First, we review the PSDPDF method to visualize the spectral characteristics of long-term seismic ambient noise (Section 1.2 and Appendix 1.A). Second, we visualize and describe numerous sources of ambient seismic noise (Section 1.3). Third, we discuss operational and research applications of the PSDPDF (Section 1.4). And finally, we conclude with software and data resources available to students and researchers (Appendix 1.C).

1.2 Visualization Methods Overview

In this section we describe the PSDPDF method using two months of seismic data recorded at station CU.BCIP at the Smithsonian Tropical Research Station on Barro Colorado Island in the Panama Canal (Figure 1.1b). The example demonstrates how the PSDPDF improves the visualization of spectrum details by mapping varying and overlapping PSDs into a probability distribution. See Appendix 1.A for a detailed description of the PSD and PDF methods. See Appendix 1.B, Table 1.1 and Figure 1.7 for station location details used for the figures throughout this chapter.

The process begins with an instrument-corrected vertical-component of motion displacement seismic time series, in this case using seismic data from channel CU.BCIP--BHZ provided in Figure 1.2a. (See Appendix 1.C for seismic station and data channel naming conventions.) A Fourier Transform (Cooley and Tukey, 1965) is applied to convert the data from the time domain into the frequency domain, the resultant PSD computed as the normalized square of the displacement spectrum (Peterson, 1993), as seen in Figure 1.2b. Figure 1.2c shows two consecutive two-hour PSDs (with a 50% overlap). Minor variations in power levels are already apparent at short (< 1 s) and long (> 10 s) periods. Figure 1.2d shows 22 PSDs computed for a complete day, January 1, 2007. Significant power variation is further observed (20–30 dB) at the short and long periods over this single day. Figure 1.2e shows 158 hourly PSDs spanning the first week of January 2007, again showing significant variation and overlap of individual PSDs at short and long periods, this overlap potentially obscuring useful detail. Figure 1.2f shows 319 hourly PSDs that span the first two weeks of January 2007. Further significant variation of PSDs at short and long periods is observed with considerable overlap of the PSDs even further obscuring detailed information. In addition, surface waves in the 10–100 s period band are observed over several hours of decaying PSD power.

Grid cells shown in Figure 1.2f represent the discretization used to construct the PSDPDF. PSDs are gathered into 1/8 octave period bins and 1 dB power bins. The PDF is computed by counting the number of PSD intersections per grid cell and then dividing each grid cell sum by the total number of PSDs (319) to obtain a percentage for each period/power bin combination (McNamara and Buland, 2004). The PSDPDF example for seismic data channel CU.BCIP--BHZ (Figure 1.1b) contains significant detail at the short and long periods that is obscured by numerous overlapping individual PSDs (Figure 1.2f) but readily visualized in the PSDPDF. Also, at long periods (> 100 s) there is an obvious bimodal distribution of power (Figure 1.1b) not observed in the overlaid PSDs (Figure 1.2f). Section 1.4 provides additional details on the source mechanism of this bimodal distribution of long-period power.

6

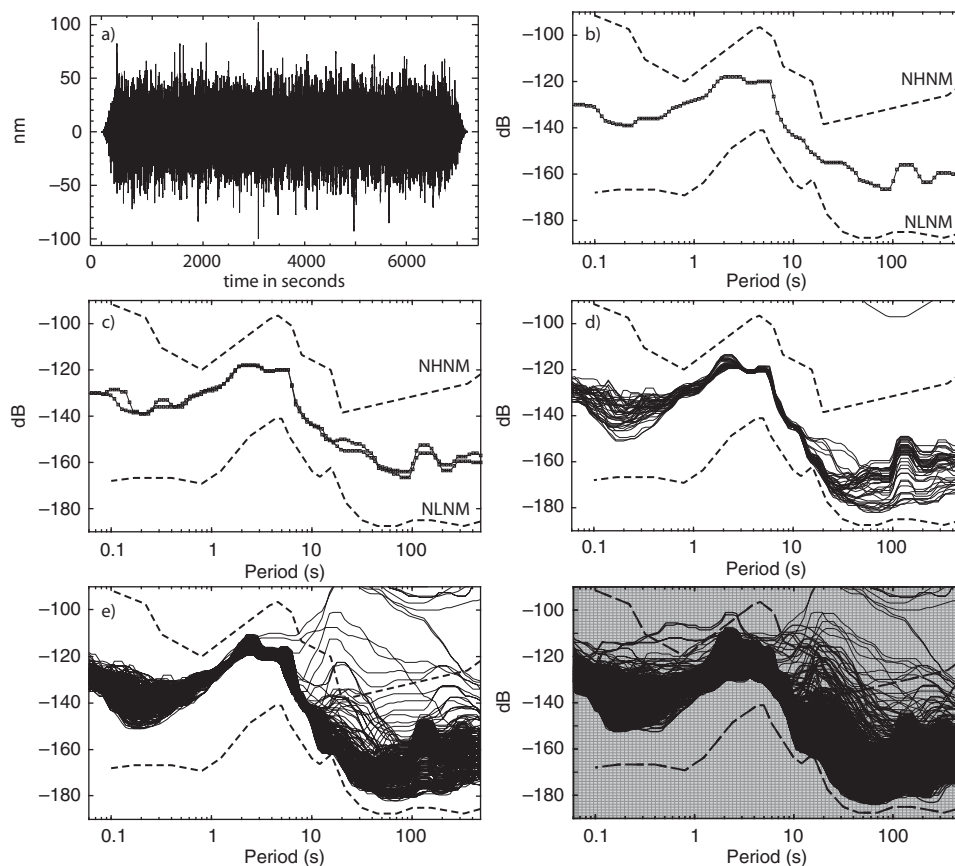
D. E. McNamara and R. I. Boaz

Figure 1.2. Example of the PSDPDF method. (a) CU.BCIP.-BHZ two-hour (7200 s) seismogram beginning on 2007-01-01 00:00:00. (b) PSD calculated for the two-hour segment in Figure 1.2a and smoothed by averaging powers over full octaves in 1/8 octave intervals, center points of averages shown. The dashed line shows the NLNM and NHNM from Peterson (1993). (c) Two continuous PSD segments. (d) PSDs for one day (22 segments). (e) PSDs for 1 week (158 segments). (f) PSDs for 2 weeks (319 segments) gridded for the PDF calculation.

1.3 PSDPDF Visualization and Applications

Long-term variation of seismic power is well visualized in a single PSDPDF plot including instrumentation problems, geographic location differences, and diurnal and seasonal variations. This can be useful for observing time-varying (i.e., diurnal and seasonal) changes in one location as well as for making comparisons between locations. Advances in instrumentation have reduced noise levels in long-period bands (> 20 s), while local noise sources which vary from station to station, such

as roads and population density, can increase short-period (< 1 s) absolute power levels and diurnal variations. Ambient noise in the mid-period band (1–20 s) is strongly affected by geographic location (mainly due to proximity of the station to coastlines) as well as the general effect of seasonal variation (McNamara and Buland, 2004).

Problems such as telemetry issues and incorrect instrument response calibrations are well visualized. For example, problems with overall sensor gain as well as transfer function shape, defined by poles and zeros, can be diagnosed by comparing the power levels versus standard baselines computed from PSDPDFs (McNamara et al., 2009). In addition, due to the probability estimate, it is possible to determine how often system problems occur, such as gaps, sensor mass re-centering, spiking, and clipping.

Optimal seismic station siting and good vault design are both important for reducing noise levels at short and long periods (McMillan, 2002; Hutt et al., 2017; Busby et al., 2013). For example, because sensors are often placed underground on concrete pads, tilt of the pad due to thermal contraction and expansion is readily observed on long-period PSDPDFs. This can usually be mitigated with a simple application of insulation, though in extreme cases deeper burial may be required to achieve low noise levels at longer periods.

In addition to seismic station and instrumentation quality control for operational applications, information can be obtained on the source characteristics of seismic ambient noise. PSDPDFs are particularly useful for the visualization of diurnal and seasonal variations of both cultural and environmental noise sources. For example, the cultural noise from cars, machinery, and even ships in the Panama Canal generally increases during the day-time hours. Seismic noise due to ocean waves has strong seasonal variation in power and has been effectively used for studies of storms and long-term decadal ocean oscillations, important for climate change monitoring (Aster et al., 2008, 2010). In the next sections we provide details on the use of PSDPDFs for studying sources of seismic ambient noise and for use in instrumentation and data quality control.

1.3.1 A Review of the Dominant Sources of Seismic Ambient Noise

Here we describe numerous examples of PSDPDFs from stations distributed throughout the various tectonic regions of the Earth (Appendix 1.B Figure 1.7, and Table 1.1). We separate noise sources into three period bands and discuss several examples of the dominant sources of seismic ambient noise within each of these bands. In general, short-period noise is dominated by human activity while mid- and long-period noise is dominated by ocean waves, but not always.

Short-Period Seismic Noise

Cultural Noise. The most common source of short-period seismic noise is from the actions of human beings at or near the surface of the Earth. This is often referred to as “cultural noise” and originates primarily from the coupling of automobile traffic and machinery energy into the solid Earth. Cultural noise propagates mainly as short-period (0.1–1 s) surface waves that attenuate within several kilometers in distance and depth. Cultural noise is often bimodal due to diurnal variations in human activity, as reflected by the fact that power levels are higher during the daytime hours and lower during the night, as well as on weekends and holidays. Figure 1.3a shows a PSDPDF from a seismic station built in a neighborhood in

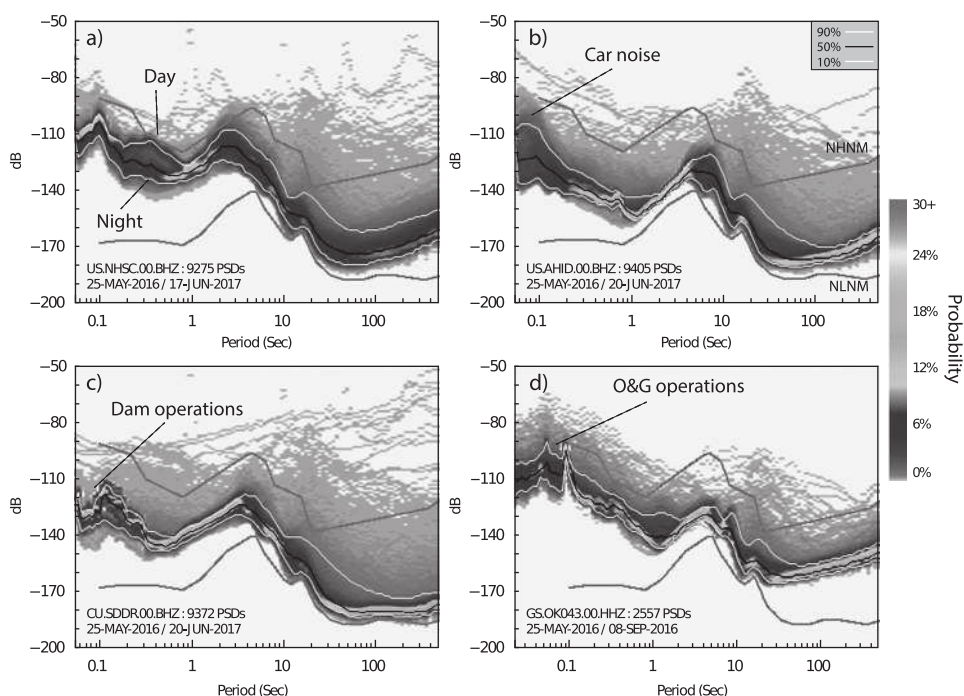


Figure 1.3. Short-period cultural noise PSDPDF examples. (a) PSDPDF of station US.NHSC.00.BHZ, constructed using 9,275 PSDs, showing bimodal, cultural, short-period noise with diurnal variation. (b) PSDPDF of station US.AHID.00.BHZ, constructed using 9,405 PSDs, showing short-period noise from car traffic on a nearby road. (c) PSDPDF of station CU.SDDR.00.BHZ, constructed using 9,372 PSDs showing short-period noise from operations at the Sabaneta Dam in the Dominican Republic. (d) PSDPDF of station GS.OK043.00.HHZ, constructed using 2,557 PSDs, showing a distinct short-period noise band from activity at oil and gas production and wastewater injection sites. (A black-and-white version of this figure appears in some formats. For the color version, please refer to the plate section.)

New Hope, South Carolina, with a clear bimodal distribution of power levels at short periods (0.1–1 s). The higher levels occur during the daytime when people are actively driving cars and operating machinery. For example, automobile traffic along a dirt road only 20 m from station US.AHID, in Auburn Hills, Idaho, creates a 30–35 dB increase in power in the 0.1 s period range and is observable in the PSDPDF (Figure 1.3b) as a region of low probability (–130 dB) at short periods (0.1–1 s).

Machinery such as diesel generators and water pumps can also have a strong influence on seismic power levels. Figure 1.3c shows station CU.SDDR, located in the high central mountains of the Dominican Republic on the grounds of the Sabaneta Dam (McNamara et al., 2006). Strong variations in short-period (0.1–0.5 s) power are clearly observed with the highest probability roughly 10 dB greater than the lower power levels. Investigation of the low power levels indicate that most occur between 1 and 3 pm local time, indicating regular periods of operational shutdown.

Often, industrial machinery will display a very sharp and distinct characteristic period band. Station GS.OK043 (Figure 1.3d) is located within one km of multiple oil and gas production and wastewater disposal sites with continuously operating pumps and generators. The seismic energy generated from this activity, near 0.1 s period, is clearly observed in the PSDPDF and suggests that there is very little downtime in the activity since low power levels in this period band are very low probability ($\sim 1\%$).

Glacier Calving. Not all short-period seismic noise is due to human activity. Station YM.BBB was located near the terminus of the Columbia Glacier on the Great Nunatak in the Prince William Sound of Alaska (O’Neel et al., 2007). Comparing visual observations of calving events and seismic energy recorded at YM.BBB, calving at the terminus was determined to generate energy in the ~ 0.5 s period band (Figure 1.4a). As the glacier retreated several kilometers from 2005 to 2008, the terminus became ungrounded (floating) causing calving energy to dissipate into the water rather than couple into the earth (Walter et al., 2010). In section 1.1 we introduced the secondary microseism, the prominent peak between 2 and 10 s period, that is generated by ocean wave action at nearby coastlines or in the deep ocean, clearly observed at all global seismic stations. The larger peak of energy between periods 0.2 and 1 s lies within the calving seismicity band (O’Neel et al., 2007) and exists only in the 2004–2005 PSDPDF. In 2008–2009, however, this energy is absent (Figure 1.4b), strongly suggesting a significant change in the calving dynamics. The 0.2–1 s period energy peak is characteristic of the tidewater glacier environment, and its disappearance indicates a decrease in seismic energy related to calving during the second deployment when the terminus was floating

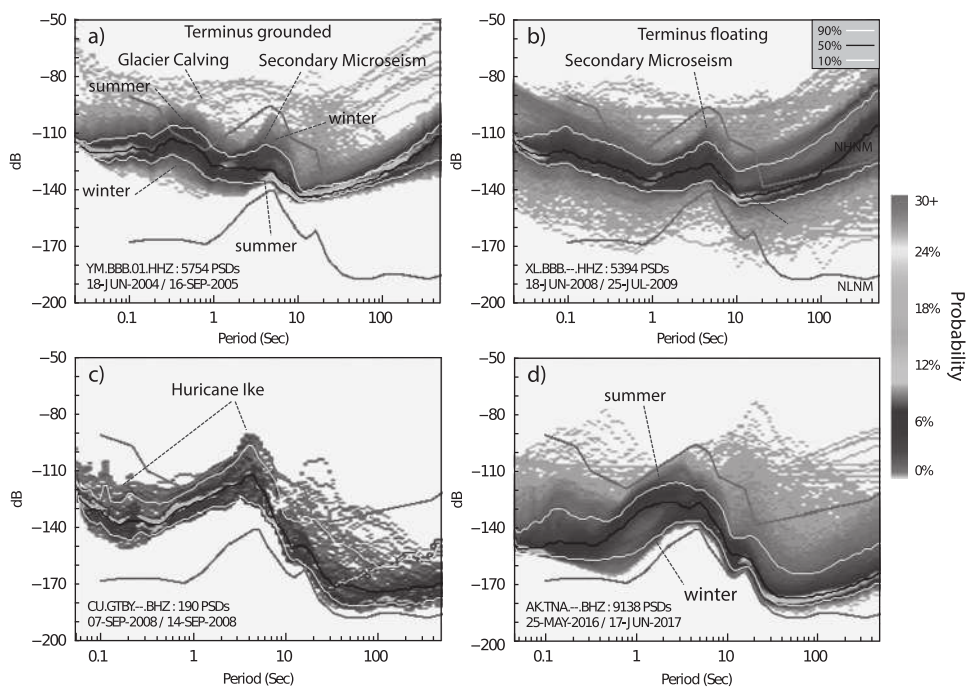


Figure 1.4. Examples of the spectral content and variation of PSDPDFs from the interaction of glaciers, storms, and sea ice with ocean wave energy. (a) PSDPDF of calving seismicity for the time period (June 18, 2004, to September 16, 2005). Station YM.BBB.01.HHZ was located at the terminus of the Columbia Glacier in the Prince William Sound of Alaska (Appendix 1.B Figure 1.7) and displays a clear power peak near 0.5 s period from calving ice. The peak near 5 s period is the secondary microseism and displays the opposite seasonal variation as the calving peak. (b) Station XL.BBB.–.HHZ occupied the same location as YM.BBB (June 18, 2008, to July 25, 2009). The 0.5 s period power peak from calving ice disappeared from the PSDPDF after the glacier terminus went from grounded to floating. (c) Hurricane Ike recorded at Guantanamo Bay seismic station (CU.GTBY.–.BHZ) as it passed by on September 7–8, 2008. Significant increases in microseism and short-period noise occurred. (d) Alaska earthquake center seismic station located on the western tip of the Seward Peninsula (AK.TNA.–.BHZ) shows the seasonal variation of Bering sea ice influence on the power level and bandwidth of the secondary microseism. (A black-and-white version of this figure appears in some formats. For the color version, please refer to the plate section.)

(Walter et al., 2010). Also, interestingly, the calving peak has the opposite seasonal variation trend than for the secondary microseism. Microseism energy in Alaska is greatest in the northern hemisphere winter months when large Pacific storms are frequent, generating large ocean wave activity, while the calving power is highest in the summer months when the temperatures are warm and the glacier is actively calving (Figure 1.4a).